Applied Thermal Engineering 221 (2023) 119796

Contents lists available at ScienceDirect

Applied Thermal Engineering

journal homepage: www.elsevier.com/locate/apthermeng

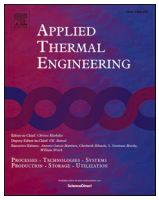

Research Paper

Parametric study of low-temperature thermal energy storage using carbon dioxide as the phase change material in pillow plate heat exchangers

Mahmood Mastani Joybari [a,*], Håkon Selvnes [b], Erling Vingelsgård [c], Alexis Sevault [b], Armin Hafner [a]

[a] Department of Energy and Process Engineering, Norwegian University of Science and Technology, Kolbjørn Hejes vei 1D, Trondheim 7491, Norway
[b] SINTEF Energy Research, Postboks 4761 Torgarden, Trondheim 7465, Norway
[c] SINTEF Ocean, Dep. Seafood Technology, Trondheim 7465, Norway

ARTICLE INFO

Keywords:
Thermal energy storage
Carbon dioxide
Phase change material
Pillow-plate heat exchanger
Parametric study
Taguchi method

ABSTRACT

Industrial low-temperature freezing applications are often batch processes, requiring a lot of energy, exerting stress on the electrical grid. To relieve this stress, thermal energy storage can be used. However, there is a lack of suitable storage material for low temperature applications (around −50 °C). Under high pressures, carbon dioxide can be used as the phase change material for storage temperatures around −55 °C. In this study, a parametric study was conducted on the design and operational parameters of an industrial-scale pillow plate heat exchanger with carbon dioxide. Two responses were selected for the analysis where R_1 considered the storage size over the phase change time (kWh/h), while R_2 indicated the cost over the storage size (USD/kWh). Using design of experiments, a total of 52 simulations were carried out to investigate the parameters under constant heat transfer surface area. Analysis of variance was then carried out followed by correlation development and optimization. It was found that regardless of the process (charging or discharging), for R_1 and R_2, the difference between refrigerant and carbon dioxide phase change temperatures followed by plate material had the highest significance. In contrast, the refrigerant flow rate had the lowest significance in almost all cases. Moreover, considering an equal weight for the responses, overall optimal conditions were determined for the processes. The recommended values for plate pitch, plate material, difference between refrigerant and carbon dioxide phase change temperatures and refrigerant flow rate were 25 mm, aluminum, 15 °C and 4 kg/s, respectively.

1. Introduction

Global warming has triggered some aspects of our energy consumption to change, including energy consumption reduction, energy efficiency enhancement, incorporating renewable energy sources, etc. All these require fundamental changes in our consumption behavior to match with the new style. Meanwhile, refrigeration systems account for about 17 % of the global electricity consumption which is expected to further increase due to global warming together with the continuous growth in refrigeration demand [1]. This means that even a small electricity consumption reduction and/or energy efficiency enhancement would have a huge impact, given the large share of refrigeration systems in global energy consumption. Food processing plants freezing meat, fish, fruits and vegetables are particularly large users of electricity since for an efficient freezing process they need low-temperature refrigeration, commonly below −40 °C [2]. Moreover, our existing electrical grids face consumption variations throughout the day with some hours having peak energy demand. To make it even worse, most renewable energy sources such as wind and solar are inherently intermittent. This makes a temporal gap between the energy supply and demand. Thermal energy storage can be used to address such issues [3]. To this end, energy can be stored during its availability to be used later when there is demand. Among thermal energy storage technologies, latent heat storage in phase change materials (PCMs) has received research momentum primarily due to its higher storage density and almost isothermal operation.

Several studies have been conducted on thermal energy storage in

Abbreviations: ANOVA, Analysis of variance; CTES, Cold thermal energy storage; DOR, Degree of freedom; GHG, Greenhouse gas; GWP, Global warming potential; HTF, Heat transfer fluid; LT, Low temperature; MS, Mean squares; ODP, Ozone depletion potential; PCM, Phase change material; PPHX, Pillow plate heat exchanger; SLE, Solid-liquid equilibrium; SS, Sum of squares.

* Corresponding author.
E-mail address: mahmood.m.joybari@ntnu.no (M. Mastani Joybari).

https://doi.org/10.1016/j.applthermaleng.2022.119796
Received 21 May 2022; Received in revised form 27 September 2022; Accepted 30 November 2022
Available online 6 December 2022

Nomenclature

A	Area (m^2)
Cp	Sensible heat capacity (J/kg °C)
E	Storage capacity (J or kWh)
h_i	Maximum inflation height (m or mm)
h_o	Center-to-center distance between pillow plates (m or mm)
H	Specific enthalpy (J/kg)
k	Thermal conductivity (W/m °C)
L	Length (m)
m	Mass (kg)
N	Number (-)
q	Liquid fraction (-)
Q	Power (W or kW)
R	Response (unit depends on the subscript)
t	Time (s)
T	Temperature (°C)
Z	Cost (USD)

Subscripts

1	Associated with the first response
2	Associated with the second response
C	Charging (solidification)
D	Discharging (melting)
l	Liquid
pass	Number of passes
pp	Pillow plate
ref	Refrigerant
s	Solid

Greek symbols

δ	Plate thickness (m or mm)
ρ	Density (kg/m^3)
Δ	Difference

refrigeration systems. It has been shown that research on the application of cold thermal energy storage (CTES) covers the entire food cold chain. Several applications have been investigated and demonstrated in food processing plants, transport and packaging, commercial refrigeration and domestic refrigeration [4,5]. Nevertheless, for low temperature refrigeration (below about −50 °C, hereinafter referred to as LT), fewer investigations are available. This topic recently received research attention due to Pfizer COVID-19 mRNA vaccine storage temperature requirements (between −60 and −80 °C) [6]. Fig. 1 shows some available commercial PCMs for LT applications (below −50 °C) which are mostly eutectic (salt hydrate/water) mixtures, which commonly suffer from subcooling. Other drawbacks of eutectic mixtures are incongruent melting, phase segregation and being corrosive to common metals used in heat exchangers [4,7]. In additions, Fig. 2 shows some candidate materials for LT thermal storage; however, they suffer from low latent heat capacity (compared to Fig. 1, note the difference in *y*-axis range). Consequently, there is a need for a suitable storage material for LT thermal energy storage.

Carbon dioxide (CO_2) is a naturally and abundantly available material. It is very commonly used as the refrigerant for LT refrigeration. As such, it can be a prime option for thermal energy storage as well. Aside from relatively high latent heat capacity, it has several advantages including low cost, molecular stability, noninflammability, low toxicity, noncorrosiveness (for most materials), zero ozone depletion potential (ODP) and low global warming potential (GWP) making it a desirable storage material for LT applications. In addition, if used as the storage material, CO_2 not only saves greenhouse gas (GHG) emissions during electricity generation, but also in itself would be a carbon storage, further lowering GHG emissions.

As such CO_2 has received attention for thermal energy storage in its solid–vapor transition (below its triple point at −56.6 °C), which is a method of achieving ultra-low temperature refrigeration. Using solid CO_2 as a source of cooling is common in many transport applications, where dry ice is loaded together with the goods to keep them at low temperature while the dry ice sublimates. The use of the solid–vapor transition of CO_2 in a cascade refrigeration system was experimentally investigated by Yamaguchi et al. [13]. Liquid CO_2 was throttled to a pressure in the range of 1.63–1.86 bar at the inlet of a test tube. By carrying out visualization tests while heating the test section, it was found that below a certain threshold of CO_2 mass flow rate, accumulation of dry ice particles occurred at the bottom of the tube which increased the risk of blocking the flow. Tests were then carried out for a cascade refrigeration system with evaporation pressure of 3.6 bar, proving that the system could achieve stable two-phase dry ice/vapor flow and continuously provide −62 °C inside the expansion tube. However, under certain conditions it was found that blocking of the

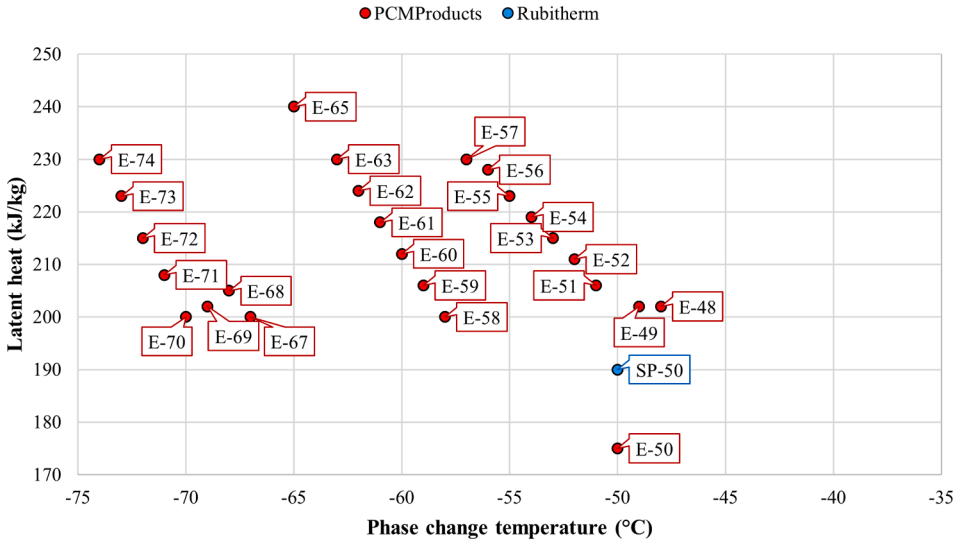

Fig. 1. Commercial PCMs for LT applications.

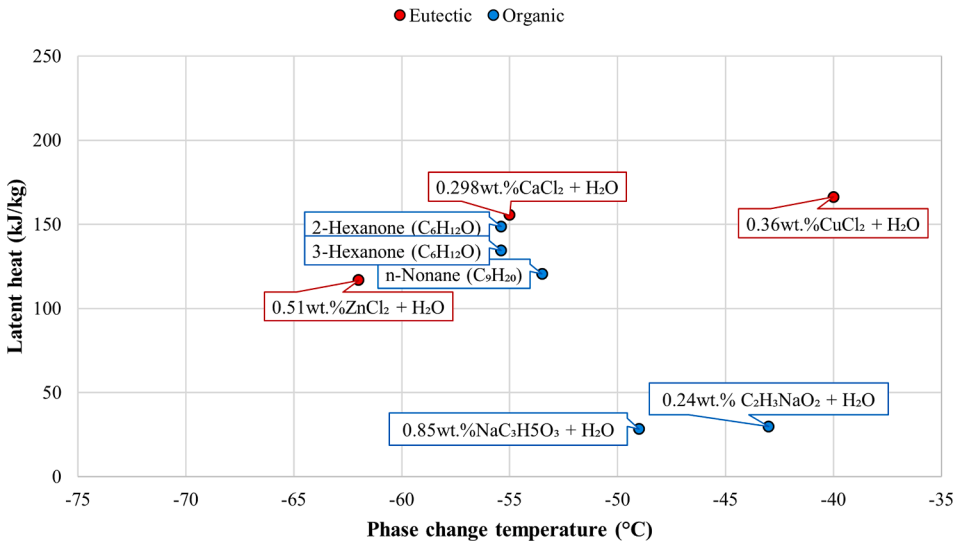

Fig. 2. Thermophysical properties of some options for LT thermal storage applications [8–12].

evaporator occurred. As a measure to reduce the risk of dry ice blocking in the evaporator tubes, the use of a swirl promoter at the inlet of the tube has been proposed [14]. It was shown by visualization tests that using the swirl promoter resulted in a more uniform dispersion of dry ice particles, improving the heat transfer, and reducing the risk of downstream blocking of the flow. The concept was further developed by proposing the use of a cyclone for collecting the dry ice particles on a bottom plate instead of the standard evaporator tube [15]. The experimental investigation showed that the conical design had the best collection efficiency compared to cylindric and non-swirling cyclones and could continuously maintain −76 °C at the bottom plate.

On the other hand, energy storage in the solid–liquid transition of CO_2 (above its triple point) has not yet received enough attention. Hafner et al. [16] proposed the concept of using CO_2 as a solid–liquid storage medium for LT energy storage in an industrial R744/R717 cascade refrigeration plant. The theoretical concept was outlined using a shell-and-tube heat exchanger integrated into the R744 circuit of the cascade system, with the CO_2 undergoing solid–liquid transition on the shell side of the heat exchanger. The calculations showed that up to 30 % reduction in electricity use was possible by avoiding inefficient part-load operation of the refrigeration plant; however, more research on the solid–liquid CO_2 transition was needed to verify the concept. Following the previous work, the same concept was applied to a CO_2 refrigeration plant utilizing plate freezers onboard a fishing vessel [17]. The numerical model predicted about 3.2 % decrease in the freezing time using the CTES, increasing the production capacity of the refrigeration system.

Several options are available for heat exchangers for instance shell and tube heat exchangers, plate heat exchangers, etc. Nevertheless, plate heat exchangers can be regarded as more suitable for thermal storage since, among others, they benefit from compact design and can withstand higher pressures. These are desirable properties for thermal storage in the solid–liquid transition of CO_2, which deals with high operating pressures. Among plate heat exchangers, pillow plate heat exchangers (PPHXs) have received attention for thermal storage applications [18]. For instance, Selvnes et al. [19] designed a lab-scale CTES unit to conduct experiments using water as the PCM. The storage was designed to have 20 horizontal pillow plates, distanced by 50 mm to store about 0.1 MWh of energy. During the tests, the refrigerant (R744) circulated through the inner channel for condensation (or evaporation), while the PCM was melting (or solidifying). The prototype had a great versatility to enable tests with other PCMs and also prevent mechanical stress during the phase change process (the plates had freedom to move up/downwards to compensate for the volume change during the PCM phase transition). They also numerically studied a 2D cross-section of the CTES unit and found that the total phase change duration for the flat and pillow plate CTES units were almost the same, making future investigations simpler using the flat plate design [20]. Besides, higher mushy zone constants (i.e., a measure that indicates the steepness of reaching zero velocity during solidification) were found to prolong the phase change process [21]. Later, Selvnes et al. [22,23] constructed an experimental setup and investigated the impact of heat transfer fluid (HTF) inlet temperature, HTF mass flow rate and plate distance on the charging (i.e., solidification) and discharging (i.e., melting) performance of the CTES unit. It was found that a smaller plate distance should be considered for covering short peaks with large magnitude. Moreover, compared to the HTF mass flow rate, the HTF temperature was found to have a more significant impact on the average PCM discharge rate, especially at higher plate distances. Similar results were reported [24,25] using a commercial organic PCM having a phase change temperature around −9 °C (i.e., RT-9HC from Rubitherm Technologies GmbH [26]). Moreover, a temperature difference of about 5 °C between the PCM phase change temperature and HTF charging temperature was found to be the best option in terms of balancing the heat transfer and energy consumption.

Sevault and Næss [27] designed and integrated a thermal storage unit to the central heating system for an office building to cover the peak heating demand. The selected PCM was organic (bio-based) with phase change temperature range of 35–37 °C (i.e., CT37 from Croda Energy Technologies [28]) to occupy the outer channel, while water circulated in the inner channel with two passes. Compared to a fin-and-tube design, utilization of a PPHX was favored due to its compactness while achieving higher heat output and durability. Previous dynamic simulations of their system showed that the unit could achieve heat input and output higher than 12 kW for more than 6 h using only 3–6 °C temperature difference between the PCM phase change temperature and HTF charging and discharging temperatures [29]. Sevault et al. [30] later built and implemented the PCM-PPHX unit and reported about a number of practical recommendations. They highlighted that one of the main cost drivers for PPHXs is the number of plates rather than their dimensions, due to their manufacturing process. It is thus more economical to maximize the size of each plate within the production abilities and minimize the number of plates needed for a given PPHX application.

Overall, despite the suitability of PPHXs for thermal storage using CO_2, no study on this topic can be found in the literature (to the best of the authors' knowledge). In addition, PPHXs have several design

parameters which should be properly investigated prior to designing a CTES unit. Different methods can be followed to conduct a parametric study. The simplest one is known as the one-at-a-time method where only one parameter is investigated while the remaining parameters remain constant. The shortcoming of this method is that it cannot consider the interaction between the parameters. In contrast, the full-factorial method individually considers all combinations of the investigated parameters. Therefore, this method is inherently time-consuming since B^A cases should be investigated for A parameters with B levels. Some other methods exist in between, which can provide the benefits of the full-factorial method while investigating some specific combination of parameters. For instance, Taguchi method is a statistical method which uses orthogonal arrays [31]. As such, the investigated conditions for each factor are balanced so that its effect can be analyzed with no interference from the other parameters [32].

In summary, the main shortcomings of the literature are: (1) limited studies on the LT thermal storage units using CO_2 as the PCM and (2) lack of a systematic parametric study on the design and operational parameters of thermal energy storage units implemented into LT refrigeration systems. Therefore, in this study, for the first time, the concept of using CO_2 as a low temperature PCM for cold thermal energy storage around −55 °C was parametrically studied for a pillow plate heat exchanger design. The rest of this paper is organized as follows: Section 2 presents the description of the proposed combination of a refrigeration plant with a thermal energy storage system. Section 3 presents the details regarding modeling and assumptions of the investigated system. In Section 4, the analysis procedure is presented followed by the results and discussions in Section 5 with the conclusions in Section 6.

2. System description

Fig. 3 shows a typical cascade refrigeration system coupled with a CTES for LT applications. In this section, the main components of the system are discussed.

2.1. Thermal storage unit

This section describes CO_2 as the PCM and a suitable heat exchanger design for that application.

2.1.1. Phase change material

The concept of LT thermal storage in the solid–liquid transition of CO_2 can be better elaborated in its pressure-enthalpy (P-h) diagram, shown in Fig. 4. In the figure, the envelope of interest for thermal energy storage is marked by a red rectangular boundary. The intention is to let CO_2 swing between the saturated solid and saturated liquid lines and avoid going beyond the liquid region. The reason is that if the temperature is rather high, then CO_2 will cross the saturated liquid line and enter the liquid–vapor region. This vapor formation is undesirable for thermal storage applications as it needs a higher volume (due to the very low density of the vapor compared to the liquid and solid phases). For instance, if the thermal storage unit is operated at 10 bar, then according to Fig. 4, temperatures above −40 °C should be avoided. Nevertheless, in practice it is challenging to adhere to this temperature requirement due to the unavoidable heat gain from the environment.

Challenges regarding the operation of the proposed system can impede using CO_2 as the PCM. Besides, the requirement of a pressurized vessel to host the PPHX and storage medium increase the cost compared to a conventional PCM that can operate at atmospheric pressure. However, it should be noted that CO_2 has already found several applications in refrigeration industry, especially for supermarket refrigeration, hot water heat pumps and industrial heat pumps. As such, its benefits and requirements are well-known which can counter its operational challenges.

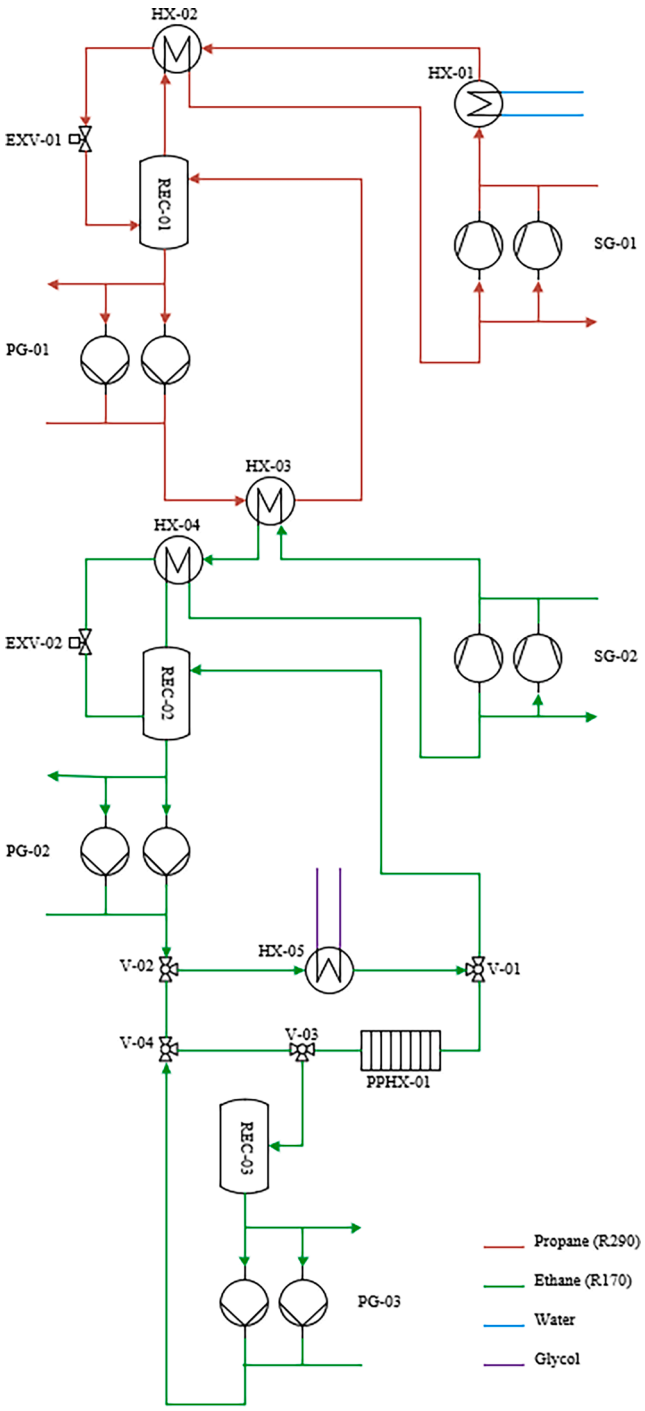

Fig. 3. Schematic circuitry of a typical cascade refrigeration system coupled with a CO_2 thermal storage unit.

2.1.2. Heat exchanger

To manufacture PPHXs, two identically thick metal plates are superimposed which are spot-welded in a specific pillow-like pattern followed by seam-welding at the edges. Thereafter, hydroforming is conducted by sending an incompressible fluid into the gap between the two plates. Then, several pillow plates are stacked together at a certain distance to create the outer channel of the PPHX. As such, the outer channel distance can be easily adjusted. For thermal storage applications, the outer channel is used for the PCM, while the refrigerant flows in the inner channel.

Note that depending on the design parameters, hydroforming

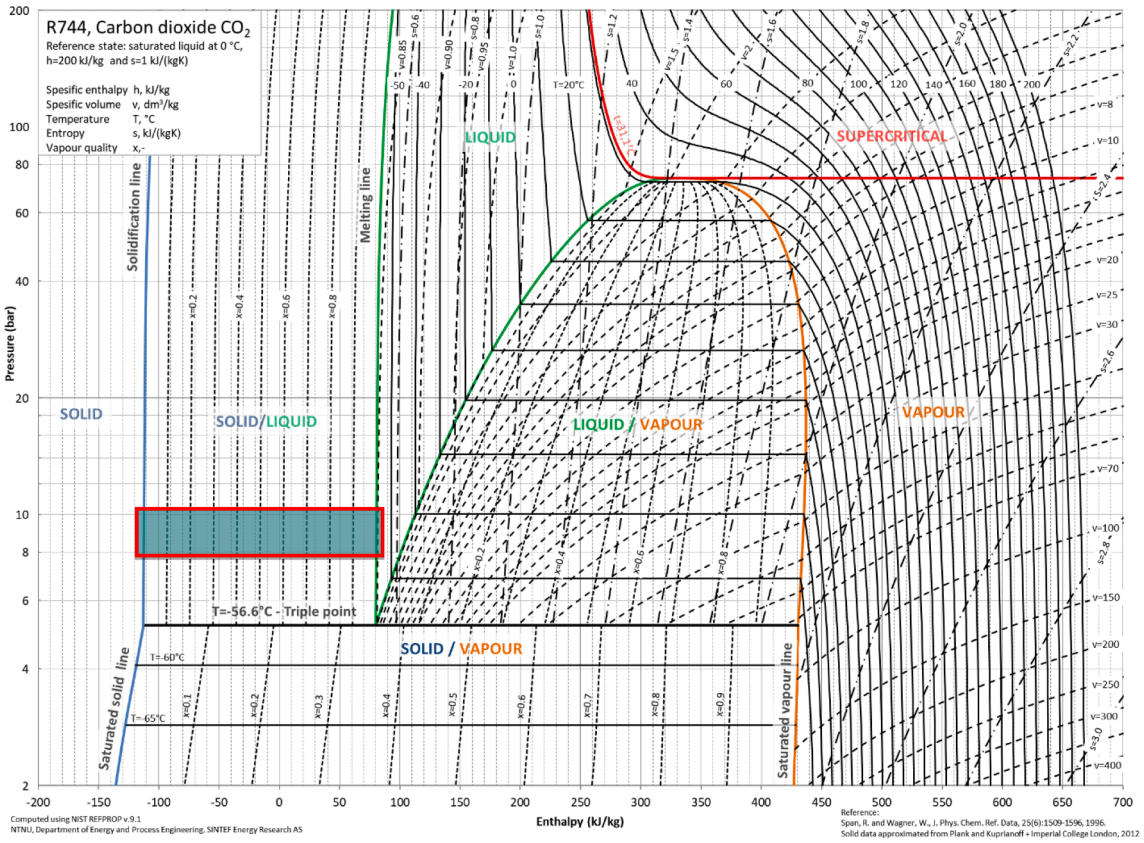

Fig. 4. CO_2 pressure-enthalpy diagram indicating the envelope considered for thermal energy storage.

pressure can go up to 70 bar [33] to achieve the desired maximum inner channel inflation height. Such high pressures are above the typical operating pressures for CO_2 as the PCM (see Fig. 4) and that is why PPHXs are suitable for such application.

2.2. Refrigerants

In order to solidify CO_2, a refrigerant with evaporation temperatures below −60 °C (see Fig. 4) is needed. Ethane (R170) is the common option for the lower stage of cascade industrial refrigeration systems due to its favorable normal boiling point of −88.8 °C [2]. Its other advantages include higher isentropic as well as volumetric efficiency together with optimal lower pressure ratio [34]. Overall, cascade R290/R170 refrigeration systems have suitable COP values especially when the evaporating and condensing temperatures are low [35].

2.3. System operation

As shown in Fig. 3, an R290/R170 cascade refrigeration system [36] was selected to elaborate the system layout and its operation. In this figure, the R290 and R170 are shown with red and green lines while blue and purple lines indicate water and glycol. In this section, the four operating modes of the system are discussed. Note that the concept can be applied to other LT applications (at around −50 °C) and the cycle in Fig. 3 was selected merely as an example to present the system layout and its operational modes. For the purpose of explaining the various operational modes, it is useful to present the various terms used for positions of the three-way valves presented in Fig. 3. The three positions are denoted “I”, “L” and “T”, where “I” indicates that the flow is directed straight through the two legs of the valve and the single leg is closed. The “L” position indicates that only one of the legs of the valve is open, meaning operation as a directional valve to one of the sides. The “T” position indicates that all legs of the valve are open, and the proportion of flow to each leg can be controlled by the opening degree of the valve towards one of the legs.

2.3.1. Mode 1: no storage

This mode is the normal system operation with no thermal storage. According to Fig. 3, hot pressurized R290 leaves suction group 1 (denoted by SG-01) and enters a water-cooled heat exchanger HX-01 which can be used for heat recovery or even connected to a heat pump unit (if needed). The condensed R290 then enters HX-02 for further subcooling prior to its expansion in EXP-01. The resulting two-phase refrigerant is then sent to a receiver (REC-01) where its vapor portion is sent to HX-02 for superheating before being sent back to SG-01. The liquid portion is then sent to a pump group (denoted by PG-01) for circulation through the cascade evaporator HX-03. The evaporated R290 is then sent back to REC-01. The lower stage of the cascade cycle which uses R170 is characteristically similar to the description above. It should be noted that as shown in Table 1, the 3-way valves V-01 and V-02 are in their “L” position in this mode.

2.3.2. Mode 2: storage charging while meeting demand

In this mode, aside from meeting the refrigeration demand in HX-05, the CTES unit (denoted by PPHX-01 in Fig. 3) is also charged. As such, the valves V-01 and V-02 are in their “T” position, while V-03 and V-04

Table 1
3-way valve positions in Fig. 3 for different operational modes.

No.	Operational mode	Valve			
		V-01	V-02	V-03	V-04
1	No storage	L	L	N/A	N/A
2	Storage charging while meeting demand	T	T	I	L
3	Storage charging only	I	I	I	L
4	Storage discharging	L	L	L	I

are in "I" and "L" positions, respectively (see Table 1). Consequently, the liquid R170 evaporates in the inner channel of the PPHX, solidifying the PCM.

2.3.3. Mode 3: Storage charging only

In this mode, there is no refrigeration load and HX-05 is bypassed by setting V-01, V-02 and V-03 in "I" position, while V-04 remains in "L" position (see Table 1). This mode can be used during nighttime when there is no refrigeration demand, to charge the storage for the next day.

2.3.4. Mode 4: storage discharging

During discharging of the CTES, all the suction groups are switched OFF to avoid power consumption during peak hours. Consequently, the CTES is used to meet the refrigeration demand in HX-05. The valves V-01, V-02 and V-03 are in their "L" position while V-04 is in "I" position. The evaporated R170 exits HX-05 and flows to PPHX-01 where it condenses by melting the PCM. The liquid R170 keeps collecting in REC-03 where it is pumped by PG-03 back to HX-05 to complete the cycle.

It should be noted that this study is focused on the storage itself (and not the rest of the system).

3. Modeling

To investigate the performance of the proposed TES systems, a dynamic simulation model was created in the object-oriented programming language Modelica [37]. The models were implemented and simulated in the programming environment Dymola 2021. The components needed to construct the model were implemented using the commercial TIL Suite package from TLK Thermo GmbH, including TIL Media thermodynamic library and TIL component library. The DASSL solver was used to solve the set of equations in the model. TIL Suite libraries are suitable for creating advanced dynamic system models of all kinds of thermal energy systems for instance automobile HVAC systems [38], heat pumps for hotels [39] and supermarket refrigeration systems [40,41]. An example of a system model for LT cascade refrigeration system for food freezing studied in this work is shown in Fig. 5. It shows a typical graphical user interface of the TIL libraries implemented in Dymola software, where the various components such as compressors, pumps, valves and heat exchangers are represented by icons. The lines between the components represent a connection to inlet/outlet conditions. Furthermore, Boolean signals or sensor signals such as pressure or temperature can be used to create control structures for controlling these systems. The documentation and equations describing heat and mass transfer in the TIL components can be found in the documentation of the TIL Suite. The focus of this study is the performance of the LT thermal energy storage using the solid–liquid transition of CO_2 as the storage medium. For this reason, it was chosen to only focus on this component (marked by the red square in Fig. 5) and connect it to inlet and outlet

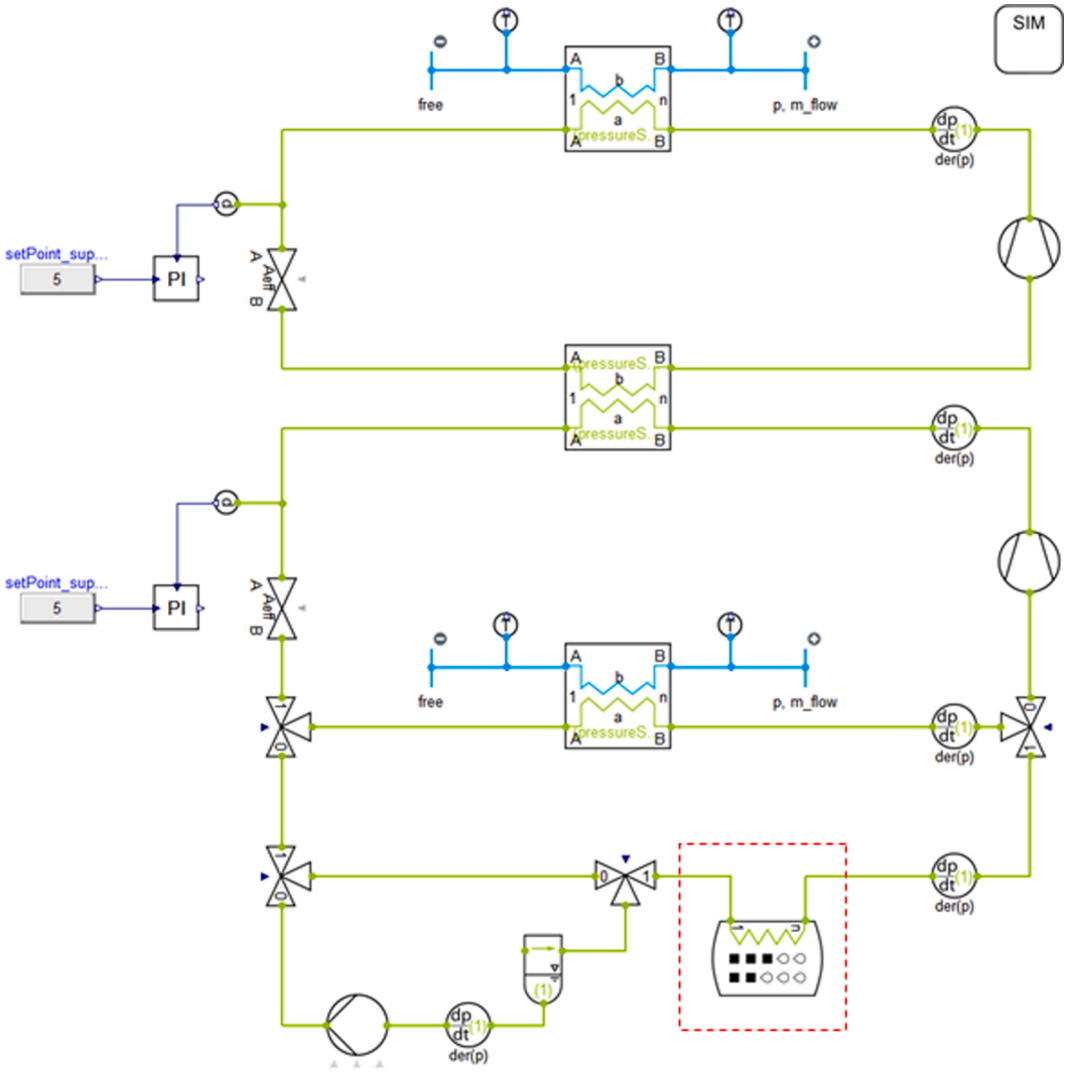

Fig. 5. Screenshot of Dymola environment indicating the main system components.

boundaries where the operating conditions could be changed according to the parametric study.

The model of the PPHX thermal energy storage unit (represented by the red square in Fig. 5) was developed and validated previously by Försterling et al. [42], and the reader is directed to that work for full details on the model structure. In the current study, the storage medium (CO_2) was represented by a solid–liquid equilibrium (SLE) cell, which was discretized in the depth direction according to the inputs from the user (see Fig. 6). The model offered flexibility in selecting both geometrical parameters for the PPHX, and the possibility to select among numerous storage media.

The thermodynamic data of the refrigerant R170 was implemented using NIST REFPROP [43]. A model entry of CO_2 as a SLE medium had to be created, specifying the thermophysical properties of both the liquid and solid phases of the material (see Table 2).

3.1. Assumptions

The following assumptions were made:

- The refrigerant flow and heat transfer in the inner channel of the PPHX were considered 1D with discretization along the heat exchanger length (e.g., *x*-direction).
- For each individual discretized cell, there was 1D heat transfer in the depth of the storage material (i.e., perpendicular to the refrigerant flow or *y*-direction) with negligible heat transfer with the neighboring cells in the *x*-direction.
- There was no heat transfer with the surroundings (i.e., negligible heat loss or heat gain).
- For melting (or solidification), the storage was initially fully solid (or liquid).
- Natural convection was neglected within the liquid PCM.

3.2. Outer channel: phase change modeling

After discretization, each PCM cell had four neighboring nodes. According to the assumptions, there was negligible heat transfer in the refrigerant flow direction (i.e., *x*-direction); thus, two nodes were technically deactivated. As such, the energy balance for heat transfer rate through each node was defined as [42]:

$$m\frac{dh}{dt} = \sum kAN\frac{2(T_n - T)}{L} \tag{1}$$

where N is the number of pillow-plates and h was determined as a function of temperature. The thermophysical properties were determined using PCM liquid-fraction (q) [42]:

$$c_p = c_{p,s} + q\left(c_{p,l} - c_{p,s}\right) \tag{2}$$

Table 2
Thermophysical properties of CO_2 in this study [44,45].

Parameter	Value		Unit
Density	1492.5 (solid)	1179.1 (liquid)	kg/m^3
Specific heat capacity	1563.6 (solid)	1950.3 (liquid)	J/kg °C
Thermal conductivity	0.0860 (solid)	0.3976 (liquid)	W/m °C
Phase change temperature	−56.46		°C
Latent heat capacity	204,930		J/kg

$$k = k_s + q(k_l - k_s) \tag{3}$$

$$\frac{1}{\rho} = \frac{1}{\rho_s} + q\left(\frac{1}{\rho_l} - \frac{1}{\rho_s}\right) \tag{4}$$

3.3. Inner channel: heat transfer and pressure drop modeling

Empirical correlations are used in the TIL library to determine heat transfer and pressure drop of the inner channel (i.e., the refrigerant). For single-phase heat transfer, the well-known Gnielinski correlation [46] was used. Regarding two-phase heat transfer, Shah Chen [47] and Shah [48] correlations were applied for evaporation and condensation, respectively. Finally, in terms of pressure drop, Swamee-Jain correlation [49] was used.

4. Methodology

Fig. 7 shows the steps and software components of the parametric study. For each scenario, first, the parameters and their levels were fed to Minitab 21 [50] to generate the test conditions using Taguchi method. Thereafter, the simulations were carried out in Dymola, where an AddOn in TIL library was used to simulate the thermal energy storage heat exchanger. The material properties for the plates and refrigerants were obtained from TIL media and NIST REFPROP [43], respectively. Once the simulations were carried out, the results were returned to Minitab 21 for further analysis and the final results were exported.

4.1. Investigated parameters

As mentioned, the thermal storage unit investigated in this study was of industrial scale. As such, a standard shipping container was considered as the size of the storage unit. Quantitatively, the overall storage dimensions were 2.3 × 6 × 2.2 m^3 (W × L × H). Therefore, the pillow-plates had dimensions of about 6 × 2.2 m^2 (L × H) and the number of pillow-plates was determined according to the container width. According to an earlier study using water/ice as the storage medium, the maximum distance between neighboring plates should not exceed 45 mm due to the increased resistance against heat transfer within the PCM

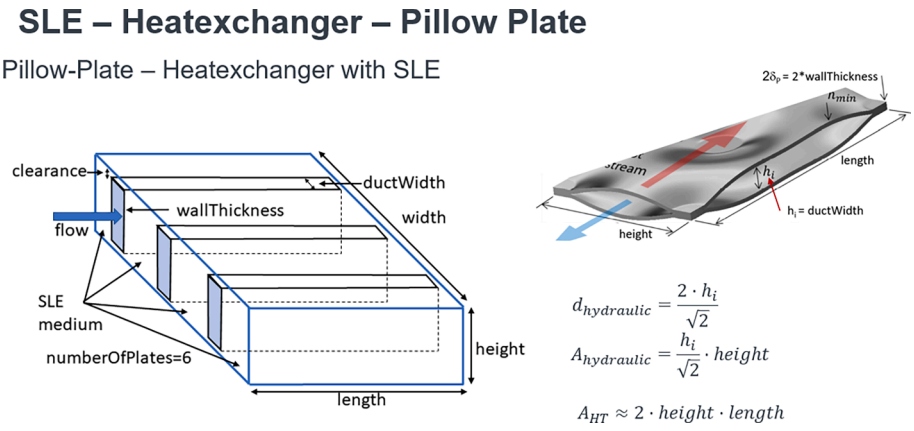

Fig. 6. Overview of the model as presented in the TIL AddOn package for thermal energy storage systems.

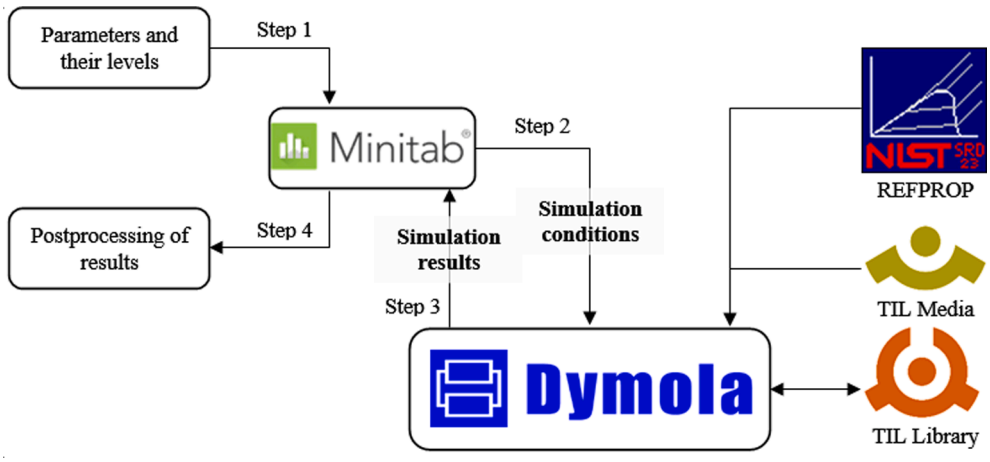

Fig. 7. Components for the parametric study in terms of software.

[23]. Consequently, 52 plates can be fit in the width of the CTES unit.

To make the analysis comprehensive, several design and operational parameters were considered in the parametric study. Table 3 shows the investigated parameters and their ranges where the total heat transfer surface area remained constant at about 1350 m^2 (according to the number of pillow-plates and their dimensions). Therefore, when the plate distance was changed, the storage width was modified accordingly so that the total heat transfer surface area remained constant.

Table 3 summarizes the parameters investigated in this study, indicating their range. Three levels were considered for all parameters so that their potential nonlinear behavior can be captured. As the table shows, all the parameters were quantitative, except for the plate material. The first five variables (i.e., A-E) were design parameters, while variables F and G were operational parameters. Parameter F indicated the difference between the phase change temperature of the PCM and the saturation temperature of the refrigerant. Note that, in this investigation the PCM phase change temperature remained constant at −56.46 °C while the refrigerant saturation temperature was determined according to parameter F.

These parameters and their levels were fed to Minitab 21 which then selected an L27 design for the parametric study which is shown Table 4. Therefore, 54 simulations were conducted, 27 for each of charging and discharging processes. Note that the refrigerant saturation temperature was determined depending on the process as well as the conditions in Table 3. The initial storage temperature was considered to be ± 5 °C above/below the phase change temperature.

4.2. Responses

To meaningfully evaluate the performance of each case, two responses were considered. The first one (denoted by R_1 in the rest of the text) was the ratio of the stored energy (in kWh) over the duration of phase change (in h) until achieving the fully charged/discharged condition:

Table 3
Parameters and their ranges considered in the parametric study.

No.	Parameter	Symbol	Level			Unit
			1	2	3	
A	Inner channel inflation height	h_i	3	5	7	mm
B	Center-to-center plate distance	h_o	25	35	45	mm
C	Number of passes	N_{pass}	1	2	3	–
D	Plate thickness	δ_{PP}	1	2	3	mm
E	Plate material	–	SS	Al	Cu	–
F	R170/PCM temperature difference	ΔT_{ref}	5	10	15	°C
G	R170 flow rate	$\dot{m}_{ref}$	4	6	8	kg/s

$$R_1 = \frac{E}{t} \tag{5}$$

The second response (denoted by R_2 in the rest of the text) was based on the cost associated with each case and was defined as the cost (in USD) over the stored energy (in kWh):

$$R_2 = \frac{Z}{E} \tag{6}$$

Both capital and operating costs were considered for each parameter. Note that it was assumed that during the discharging process, the temperature difference between the refrigerant condensation temperature and the PCM phase change temperature had zero cost.

Defining the responses as shown in Equations (5) and (6) it was possible to consider two opposing aspects of the system. In other words, since maximizing one of these responses inherently minimizes the other, their combination would be a trade-off, reflecting the practical requirements of a CTES unit in terms of stored energy, phase change duration and cost.

5. Results and discussion

In this section, the results are analyzed using Taguchi method, followed by correlation development and obtaining optimal conditions as well as their verification.

5.1. Analysis of results

In Taguchi method, the analysis is conducted in terms of a parameter known as signal-to-noise ratio (S/N). As its name implies, this parameter indicates the contribution of desired results (i.e., signal) over undesired ones (i.e., noise) [51]. In addition, it facilitates the analysis since unlike individual responses which might need to be minimized, maximized or nominally set, S/N should always be maximized:

$$S/N = -10\log\left(R^2\right) For\ minimization \tag{7}$$

$$S/N = -10\log\left(\frac{1}{R^2}\right) For\ maximization \tag{8}$$

where R is the individual response.

A summary of the responses and their S/N values are tabulated in Table 5. For the latter, the main effect plots are shown in Fig. 8 and Fig. 9 for the charging and discharging processes, respectively. Such data can be used to rank the parameters in terms of their contribution (presented in Section 5.2). In these figures, the impact of each parameter on each response can be understood where a higher variation of S/N ratio indicates higher significance. As an example, for R_2 in the charging process

Table 4
The selected L27 design for the parametric study.

Run	Level							Run	Level							Run	Level						
	A	B	C	D	E	F	G		A	B	C	D	E	F	G		A	B	C	D	E	F	G
1	1	1	1	1	1	1	1	**10**	2	1	2	3	1	2	3	**19**	3	1	3	2	1	3	2
2	1	1	1	1	2	2	2	**11**	2	1	2	3	2	3	1	**20**	3	1	3	2	2	1	3
3	1	1	1	1	3	3	3	**12**	2	1	2	3	3	1	2	**21**	3	1	3	2	3	2	1
4	1	2	2	2	1	1	1	**13**	2	2	3	1	1	2	3	**22**	3	2	1	3	1	3	2
5	1	2	2	2	2	2	2	**14**	2	2	3	1	2	3	1	**23**	3	2	1	3	2	1	3
6	1	2	2	2	3	3	3	**15**	2	2	3	1	3	1	2	**24**	3	2	1	3	3	2	1
7	1	3	3	3	1	1	1	**16**	2	3	1	2	1	2	3	**25**	3	3	2	1	1	3	2
8	1	3	3	3	2	2	2	**17**	2	3	1	2	2	3	1	**26**	3	3	2	1	2	1	3
9	1	3	3	3	3	3	3	**18**	2	3	1	2	3	1	2	**27**	3	3	2	1	3	2	1

Table 5
Summary of responses as well as their S/N ratios for charging and discharging processes.

Run	Level							Charging				Discharging			
	A	B	C	D	E	F	G	R_{1C}	R_{2C}	S/N_{1C}	S/N_{2C}	R_{1D}	R_{2D}	S/N_{1D}	S/N_{2D}
1	1	1	1	1	1	1	1	82.3	105.7	38.30	−40.48	221.4	25.3	46.91	−28.05
2	1	1	1	1	2	2	2	175.0	95.4	44.86	−39.59	506.9	7.3	54.10	−17.29
3	1	1	1	1	3	3	3	270.1	162.5	48.63	−44.22	783.2	49.0	57.88	−33.80
4	1	2	2	2	1	1	1	56.6	121.1	35.06	−41.66	149.0	36.3	43.46	−31.21
5	1	2	2	2	2	2	2	122.3	99.5	41.75	−39.95	355.5	9.7	51.02	−19.75
6	1	2	2	2	3	3	3	188.9	190.3	45.53	−45.59	550.7	70.3	54.82	−36.93
7	1	3	3	3	1	1	1	43.2	131.1	32.70	−42.35	112.3	43.2	41.01	−32.70
8	1	3	3	3	2	2	2	94.0	102.6	39.46	−40.22	273.8	11.4	48.75	−21.11
9	1	3	3	3	3	3	3	145.3	207.0	43.24	−46.32	424.4	82.7	52.56	−38.35
10	2	1	2	3	1	2	3	241.3	199.7	47.65	−46.01	497.6	90.4	53.94	−39.12
11	2	1	2	3	2	3	1	427.8	122.6	52.63	−41.77	1114.9	18.7	60.94	−25.42
12	2	1	2	3	3	1	2	140.4	305.8	42.94	−49.71	381.8	183.7	51.64	−45.28
13	2	2	3	1	1	2	3	123.6	113.4	41.84	−41.09	336.9	20.0	50.55	−26.04
14	2	2	3	1	2	3	1	194.9	106.2	45.79	−40.52	559.1	5.0	54.95	−13.99
15	2	2	3	1	3	1	2	62.1	125.1	35.86	−41.94	179.6	37.8	45.09	−31.55
16	2	3	1	2	1	2	3	92.9	127.2	39.36	−42.09	247.3	29.9	47.86	−29.52
17	2	3	1	2	2	3	1	148.9	109.1	43.46	−40.75	431.4	6.9	52.70	−16.80
18	2	3	1	2	3	1	2	47.4	152.5	33.52	−43.66	137.8	57.8	42.78	−35.24
19	3	1	3	2	1	3	2	432.7	170.8	52.72	−44.65	909.3	56.7	59.17	−35.07
20	3	1	3	2	2	1	3	152.1	93.4	43.64	−39.41	400.9	15.4	52.06	−23.78
21	3	1	3	2	3	2	1	308.7	229.9	49.79	−47.23	795.2	114.9	58.01	−41.21
22	3	2	1	3	1	3	2	246.7	173.7	47.85	−44.79	555.3	58.4	54.89	−35.33
23	3	2	1	3	2	1	3	86.4	98.0	38.73	−39.83	238.9	16.8	47.56	−24.53
24	3	2	1	3	3	2	1	179.0	235.1	45.06	−47.42	491.3	118.4	53.83	−41.47
25	3	3	2	1	1	3	2	150.4	120.0	43.54	−41.58	413.5	14.9	52.33	−23.48
26	3	3	2	1	2	1	3	48.7	95.6	33.75	−39.61	140.6	10.8	42.96	−20.68
27	3	3	2	1	3	2	1	99.9	121.5	40.00	−41.69	287.9	27.7	49.19	−28.83

(indicated by R_{2C} in Fig. 8), parameter G (i.e., refrigerant mass flow rate) had the lowest impact. On the other hand, the highest impact belonged to parameter E (i.e., plate material). This is logical since the cost of the plate material differs significantly between stainless steel, aluminum and copper and its impact on the CTES unit cost is significant. Further analysis is provided in the following sections.

5.2. Ranking of parameters

The S/N ratio values presented in Table 5 can be further analyzed to rank the parameters. The ranking is shown in Table 6 and Table 7 for charging and discharging processes, respectively. The tables show that regardless of the process (i.e., charging or discharging), for R_1 and R_2, parameters F (i.e., R170/PCM temperature difference) and E (i.e., plate material) had the highest ranking, respectively. On the other hand, parameter G (i.e., R170 flow rate) had the lowest ranking in almost all cases, except for R_{2D} where parameter C (i.e., number of passes) had the lowest ranking.

5.3. Analysis of variance

Analysis of variance (ANOVA) is a mathematical procedure to identify the contribution and significance of each parameter [52]. Consequently, they can be ranked in terms of their significance and those parameters with less significance (if they exist) can be removed from further analysis [32].

Table 8 and Table 9 show ANOVA results for the charging and discharging processes, respectively. In these tables, higher values under the column F-value indicate higher significance for each parameter. For instance, according to the tables, for R_1 the highest significance belonged to parameter F followed by B (i.e., R170/PCM temperature difference and center-to-center plate distance, respectively). On the other hand, for the discharging process, parameter E had the highest significance followed by D (i.e., plate material and plate thickness, respectively). Overall, the results are in line with those presented in Table 6 and Table 7.

5.4. Regression

In the next step, correlations were developed for each response using regression analysis. Such correlations have practical application for instance for design, prediction and optimization. Note that in the regression analysis, first, all the possible interactions among variables were considered. Then, stepwise backward elimination regression was

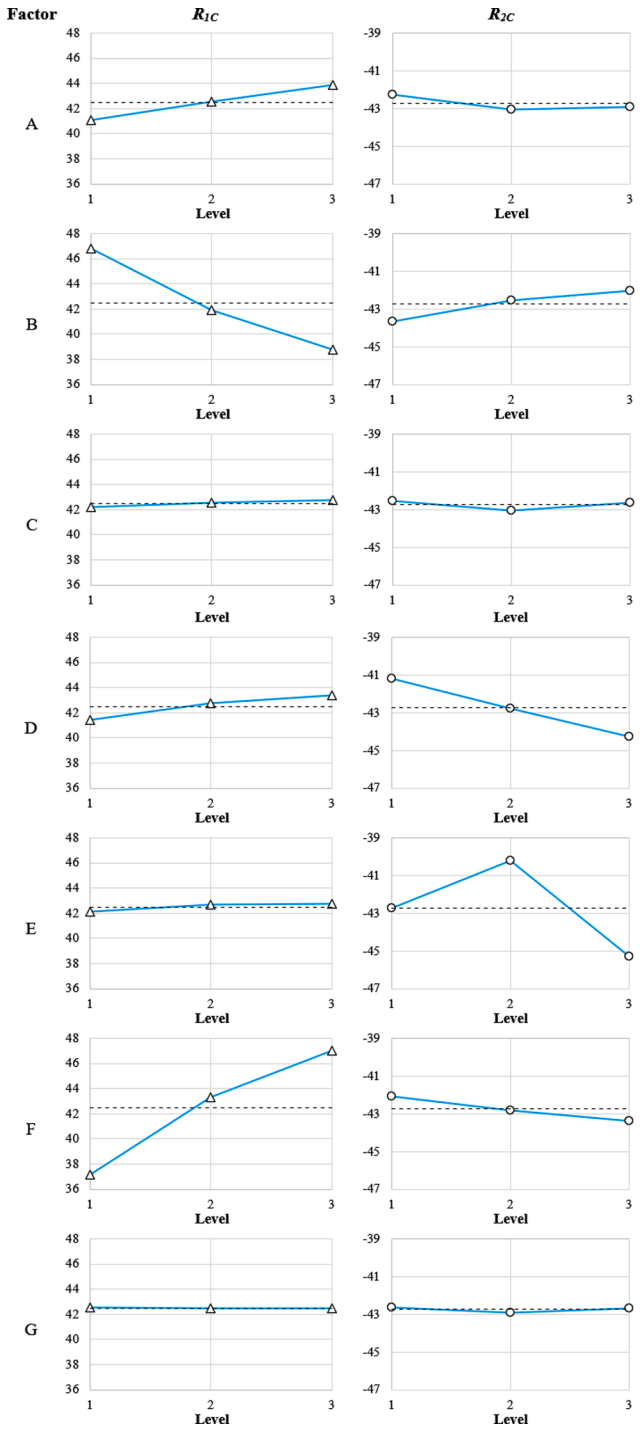

Fig. 8. Main effect plots for the S/N ratios (charging process).

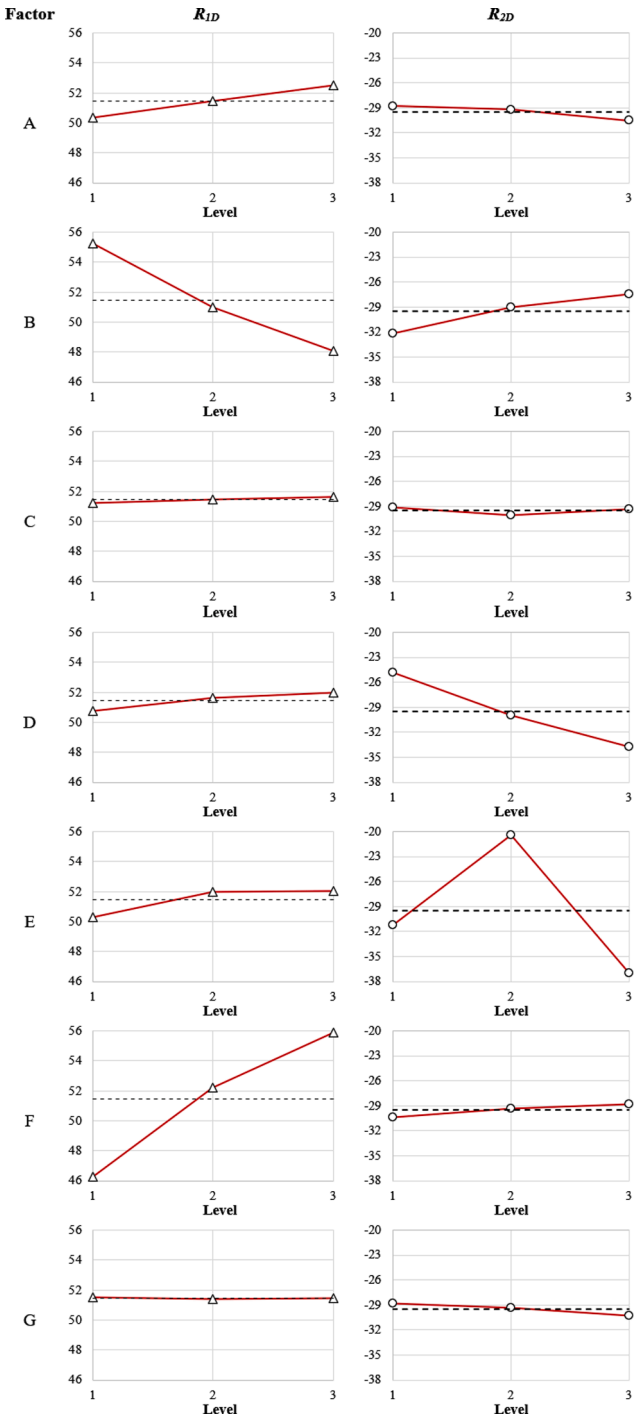

Fig. 9. Main effect plots for the S/N ratios (discharging process).

conducted (considering 0.1 for alpha). In other words, in each step, the least significant parameter (or interaction) was removed until all the remaining parameters were significant (i.e., their p-values were less than or equal to the considered alpha value).

The following correlations were developed for the charging process:

$$R_{1C} = 127.3 - 33.7A - 1.38B - 108.2C + 46.23D + 42.81F - 27.23G + R^2 = 98.89\% \\ 24.17A \times C - 0.7512B \times F + 0.626B \times G \quad (9)$$

Table 6
Change in S/N ratio for each parameter and their ranking (charging process).

Parameter	R_{1C}						
	A	B	C	D	E	F	G
Level 1	41.06	46.80	42.20	41.40	42.11	37.17	42.53
Level 2	42.56	41.94	42.54	42.76	42.67	43.31	42.50
Level 3	43.90	38.78	42.78	43.36	42.73	47.04	42.49
Delta	2.84	8.02	0.59	1.96	0.61	9.88	0.05
Rank	3	2	6	4	5	1	7
Parameter				R_{2C}			
	A	B	C	D	E	F	G
Level 1	−42.26	−43.67	−42.54	−41.19	−42.75	−42.07	−42.65
Level 2	−43.06	−42.53	−43.06	−42.78	−40.18	−42.81	−42.90
Level 3	−42.91	−42.03	−42.64	−44.27	−45.31	−43.36	−42.68
Delta	0.80	1.64	0.53	3.08	5.13	1.28	0.25
Rank	5	3	6	2	1	4	7

Table 7
Change in S/N ratio for each parameter and their ranking (discharging process).

Parameter	R_{1D}						
	A	B	C	D	E	F	G
Level 1	50.05	54.96	50.95	50.44	50.01	45.94	51.22
Level 2	51.16	50.68	51.14	51.32	51.67	51.92	51.08
Level 3	52.22	47.79	51.35	51.68	51.75	55.58	51.13
Delta	2.17	7.17	0.40	1.24	1.74	9.64	0.14
Rank	3	2	6	5	4	1	7
Parameter				R_{2D}			
	A	B	C	D	E	F	G
Level 1	−28.80	−32.11	−29.11	−24.86	−31.17	−30.34	−28.85
Level 2	−29.22	−28.98	−30.08	−29.94	−20.37	−29.37	−29.34
Level 3	−30.49	−27.41	−29.31	−33.70	−36.96	−28.80	−30.31
Delta	1.69	4.70	0.97	8.84	16.59	1.54	1.45
Rank	4	3	7	2	1	5	6

$$R_{2C} = \begin{cases} \exp(4.721 - 0.00945B + 0.1918D + 0.01479F) & For: SS \\ \exp(4.729 - 0.00945B + 0.0403D + 0.01479F) & For: Al \;\; R^2 \\ \exp(4.801 - 0.00945B + 0.2993D + 0.01479F) & For: Cu \end{cases} = 93.63\% \tag{10}$$

Note that in Equation (9), three interactions were found significant for R_{1C} (i.e., A × C, B × F and B × G), while parameter E (i.e., plate material) was found to be insignificant. On the other hand, in Equation (10), plate material was significant and as such, three different correlations were developed for each plate material. Note that the best regression was found for exponential functions. Similarly, for the discharging process, the following correlations were developed:

$$R_{1D} = 311 - 9.8A - 8.14B - 212.7C + 83.5D + 125.9F - 92.8G + 46.7A \times C - 5.99A \times F - 1.541B \times F + 1.794B \times G \tag{11}$$

$$R_{2D} = \begin{cases} \exp(3.084 + 0.0486A - 0.02706B + 0.5676D + 0.01772F + 0.0418G) & For: SS \\ \exp(2.243 + 0.0486A - 0.02706B + 0.3666D + 0.01772F + 0.0418G) & For: Al \;\; R^2 = 98.13\% \\ \exp(3.699 + 0.0486A - 0.02706B + 0.5932D + 0.01772F + 0.0418G) & For: Cu \end{cases} \tag{12}$$

Again, in Equation (11) some interactions were found to be significant for R_{1D} (i.e., A × C, A × F, B × F and B × G). Regarding Equation (12), the exponential correlations had the best performance with the number of parameters more than that of Equation (10). This was (as mentioned earlier) due to the fact that parameter F (i.e., R170/PCM temperature difference) had zero cost during the discharging process. Consequently, the significance of the other parameters was increased, and more terms appeared in Equation (12) compared to Equation (10).

Determination coefficient (i.e., R^2) is a common statistical measure to verify the goodness of the fit. In Equations (9)-(12), the minimum R^2 value was 93.63 %, which is above the conventionally acceptable threshold of 90 %. To further verify the performance of these correlations, Fig. 10 shows the parity plots for these correlations (i.e., correlation predictions versus simulation results). The figures graphically show the proper performance of each correlation.

5.5. Optimal condition

Based on the results obtained from ANOVA, the optimal conditions were identified for each individual response as shown in Table 10. Note that the term "Any" indicates those parameters which were found to be insignificant by ANOVA results. In such cases, the value in front of the term "Any" shows the value considered in this study which was obtained from the neighboring column in Table 10 for each process. These values were used to verify the performance of that optimal conditions.

Regarding R_1, the first column (denoted by "Optimal$_{1C}$" and "Optimal$_{1D}$") shows that the optimal condition is the same regardless of the process. Regarding the parameters with the highest ranking in Table 6

Table 8
The results of analysis of variance (charging process).

		R_{1C}				
Parameter	Name	DOF *	SS$	MS#	F-value	p-value
A	Inner channel inflation height	2	36.278	18.139	278.53	0.000
B	Center-to-center plate distance	2	293.466	146.733	2253.16	0.000
C	Number of passes	2	1.569	0.784	12.05	0.001
D	Plate thickness	2	18.226	9.113	139.93	0.000
E	Plate material	2	2.081	1.041	15.98	0.000
F	R170/PCM temperature difference	2	447.592	223.796	3436.50	0.000
G	R170 flow rate	2	0.010	0.005	0.08	0.928
	Error	12	0.781	0.065		
	Total	26	800.003			
		R_{2C}				
Parameter	Name	DOF *	SS$	MS#	F-value	p-value
A	Inner channel inflation height	2	3.236	1.6179	0.84	0.454
B	Center-to-center plate distance	2	12.736	6.3679	3.32	0.071
C	Number of passes	2	1.409	0.7044	0.37	0.700
D	Plate thickness	2	42.616	21.3082	11.12	0.002
E	Plate material	2	118.238	59.1192	30.84	0.000
F	R170/PCM temperature difference	2	7.479	3.7395	1.95	0.185
G	R170 flow rate	2	0.326	0.1630	0.09	0.919
	Error	12	23.001	1.9167		
	Total	26	209.041			

* Degree of freedom.
$ Sum of squares.
# Mean squares.

Table 9
The results of analysis of variance (discharging process).

		R_{1D}				
Parameter	Name	DOF *	SS$	MS#	F-value	p-value
A	Inner channel inflation height	2	21.149	10.574	23.30	0.000
B	Center-to-center plate distance	2	234.125	117.063	257.97	0.000
C	Number of passes	2	0.734	0.367	0.81	0.468
D	Plate thickness	2	7.342	3.671	8.09	0.006
E	Plate material	2	17.349	8.674	19.12	0.000
F	R170/PCM temperature difference	2	426.279	213.139	469.69	0.000
G	R170 flow rate	2	0.086	0.043	0.10	0.910
	Error	12	5.445	0.454		
	Total	26	712.510			
		R_{2D}				
Parameter	Name	DOF *	SS$	MS#	F-value	p-value
A	Inner channel inflation height	2	13.90	6.949	2.37	0.135
B	Center-to-center plate distance	2	103.14	51.568	17.62	0.000
C	Number of passes	2	4.70	2.349	0.80	0.471
D	Plate thickness	2	354.63	177.317	60.59	0.000
E	Plate material	2	1276.28	638.139	218.06	0.000
F	R170/PCM temperature difference	2	10.89	5.443	1.86	0.198
G	R170 flow rate	2	9.84	4.919	1.68	0.227
	Error	12	35.12	2.926		
	Total	26	1808.48			

* Degree of freedom.
$ Sum of squares.
# Mean squares.

and Table 7, the optimal value for the difference between the refrigerant and PCM phase change temperatures (i.e., parameter F, ranked first) was found to be 15 °C which is logical since higher temperature difference means higher driving force for heat transfer resulting in a shorter phase change process. In addition, the optimal center-to-center plate distance (i.e., parameter B, ranked second) was found to be 25 mm. This is in line with the mechanism of heat transfer within the PCM as higher distance means thicker PCM and in turn, higher resistance against heat transfer.

Regarding R_2, the second column (denoted by "Optimal$_{2C}$" and "Optimal$_{2D}$") indicates some difference between the optimal conditions for the two processes. Nevertheless, the parameter with the highest ranking for both processes was the plate material (i.e., parameter E in Table 6 and Table 7) whose optimal material was found to be aluminum. Although the cost of aluminum is comparable to that of stainless steel, the reason for the finding was that using stainless steel increased other operational costs of the system (primarily due to the higher resistance against heat transfer as compared to aluminum). Overall, the tensile strength of aluminum is lower than stainless steel, but due to being much lighter, the strength to weight ratio is higher for aluminum. Regarding corrosion, compared to stainless steel, aluminum is more resistant against oxidation at the presence of water/moisture. However, aluminum can be subject to corrosion in the presence of salts, commonly found in many low-temperature PCMs (salt-water mixtures). In this study, pure carbon dioxide was considered as the PCM which is compatible with aluminum in terms of corrosion.

In addition, Table 10 shows an "Overall" optimal condition which was obtained by simultaneously considering both responses with equal weights (i.e., 50 % weight for each response). This was considered due to the lack of any recommendation for the weight in the literature. The table shows that regardless of the process, under the overall optimal condition, the recommended value for center-to-center plate distance, plate material, R170/PCM temperature difference and R170 flow rate were 25 mm, aluminum, 15 °C and 4 kg/s, respectively. The latter two are in line with the literature which found the best performance for the highest driving force (i.e., R170/PCM temperature difference) and relatively negligible impact of refrigerant mass flow rate (as long as proper distribution of refrigerant is ensured within the pillow plate) [25]. Other parameters should be selected according to the process, as shown in Table 10.

Overall, since none of the obtained optimal combinations have been investigated earlier (see Table 4), they had to be simulated and further verified to check if they can (at least) outperform the results obtained earlier in Table 5.

5.6. Verification

Using the optimal conditions in Table 10, six more simulations were carried out to verify their optimality. The results are tabulated in Table 11 which are further analyzed in this section.

Fig. 11 compares the results obtained using the investigated L27 design (see Table 4) with those obtained for the optimal conditions

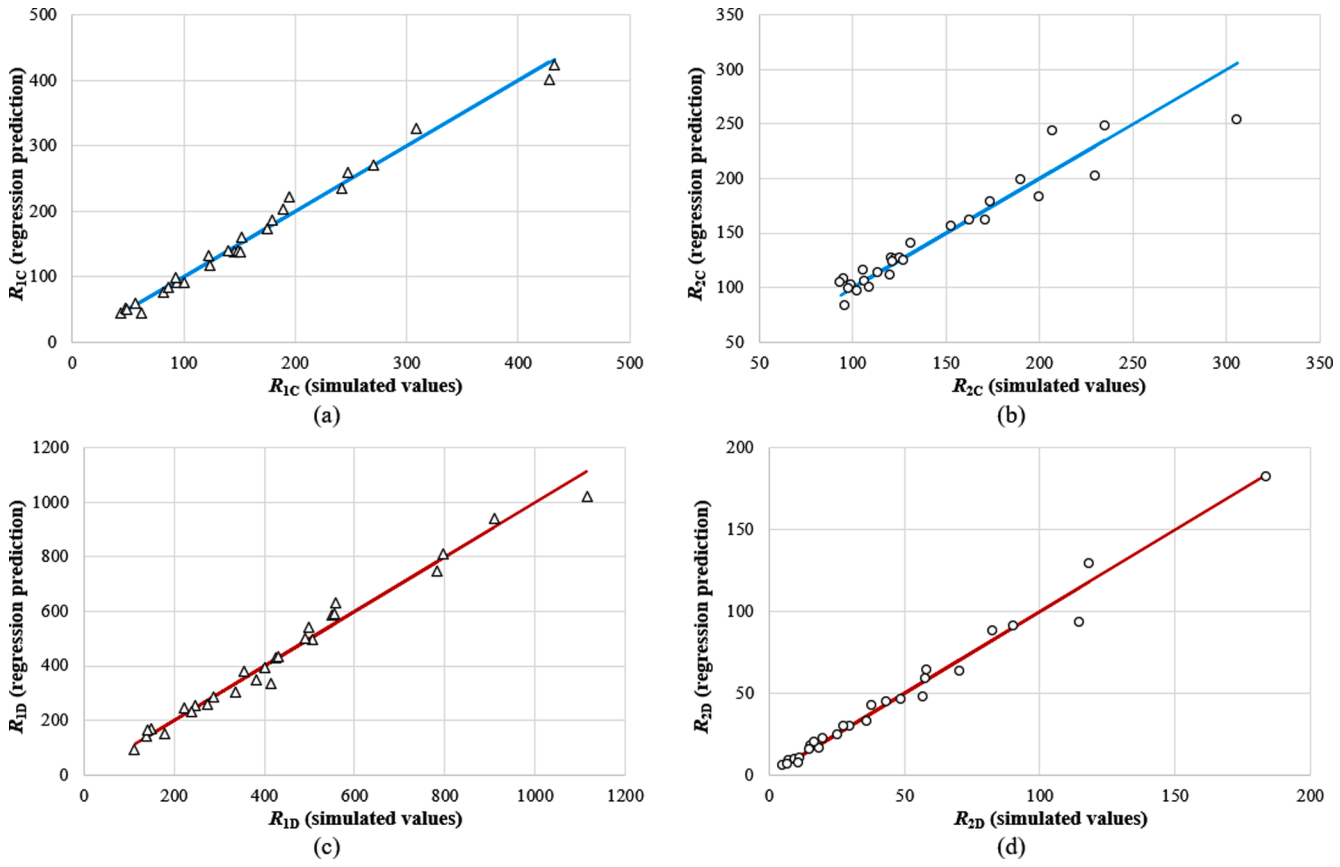

Fig. 10. Parity plots for the correlations developed for (a and b) the charging process and (c and d) the discharging process.

Table 10
The optimal conditions obtained for each individual response together with the overall.

Parameter	Name	Optimal conditions (charging)		
		$Optimal_{1C}$	$Optimal_{2C}$	Overall
A	Inner channel inflation height	7	Any (7)	7
B	Center-to-center plate distance	25	45	25
C	Number of passes	3	Any (3)	3
D	Plate thickness	3	1	1
E	Plate material	Any (Al)	Al	Al
F	R170/PCM temperature difference	15	5	15
G	R170 flow rate	4	Any (4)	4
Already investigated? (see Table 4)		No	No	No
Parameter	**Name**	**Optimal conditions (discharging)**		
		$Optimal_{1D}$	$Optimal_{2D}$	Overall
A	Inner channel inflation height	7	3	3
B	Center-to-center plate distance	25	45	25
C	Number of passes	3	Any (1)	1
D	Plate thickness	3	1	3
E	Plate material	Any (Al)	Al	Al
F	R170/PCM temperature difference	15	15	15
G	R170 flow rate	4	4	4
Already investigated? (see Table 4)		No	No	No

(shown in Table 10). The blue and red horizontal lines in the figure show the performance of the corresponding optimal case for the charging and discharging processes, respectively.

As mentioned earlier, the objective for R_1 (dealing with the storage size over phase change duration) was to maximize its performance. According to Fig. 11a, regardless of the process, the values obtained for "Optimal 1" outperformed all other results, confirming its optimal performance. On the other hand, R_2 (dealing with the CTES unit cost over its storage size) should be minimized. According to Fig. 11b, regardless of the process, "Optimal 2" had the lowest values compared to all the rest, indicating its optimal performance.

In these figures, the performance of the "Overall" optimal condition can also be verified. In Fig. 11a, the "Overall" optimal condition performed acceptably close to the possible maximization (presented by "Optimal 1"). Note that "Optimal 1" ignores the cost and inherently goes in the opposite direction compared to the cost. As such, it makes sense for the "Overall" optimal condition to have somewhat less performance compared to the dedicated "Optimal 1" scenario. Similarly, in Fig. 11b, the "Overall" optimal condition had comparably close performance to that of "Optimal 2" for the same reasons discussed earlier.

Table 11
The results for verification tests on the obtained optimal conditions (Table 10).

Response	Optimal conditions (charging)		
	$Optimal_{1C}$	$Optimal_{2C}$	Overall
R_{1C} (kWh/h)	659.5	48.6	389.7
R_{2C} (USD/kWh)	120.1	85.0	107.3
Response	**Optimal conditions (discharging)**		
	$Optimal_{1D}$	$Optimal_{2D}$	Overall
R_{1D} (kWh/h)	1317.5	378.8	948.4
R_{2D} (USD/kWh)	19.8	4.5	17.7

6. Conclusion

Few studies have been conducted on low-temperature thermal

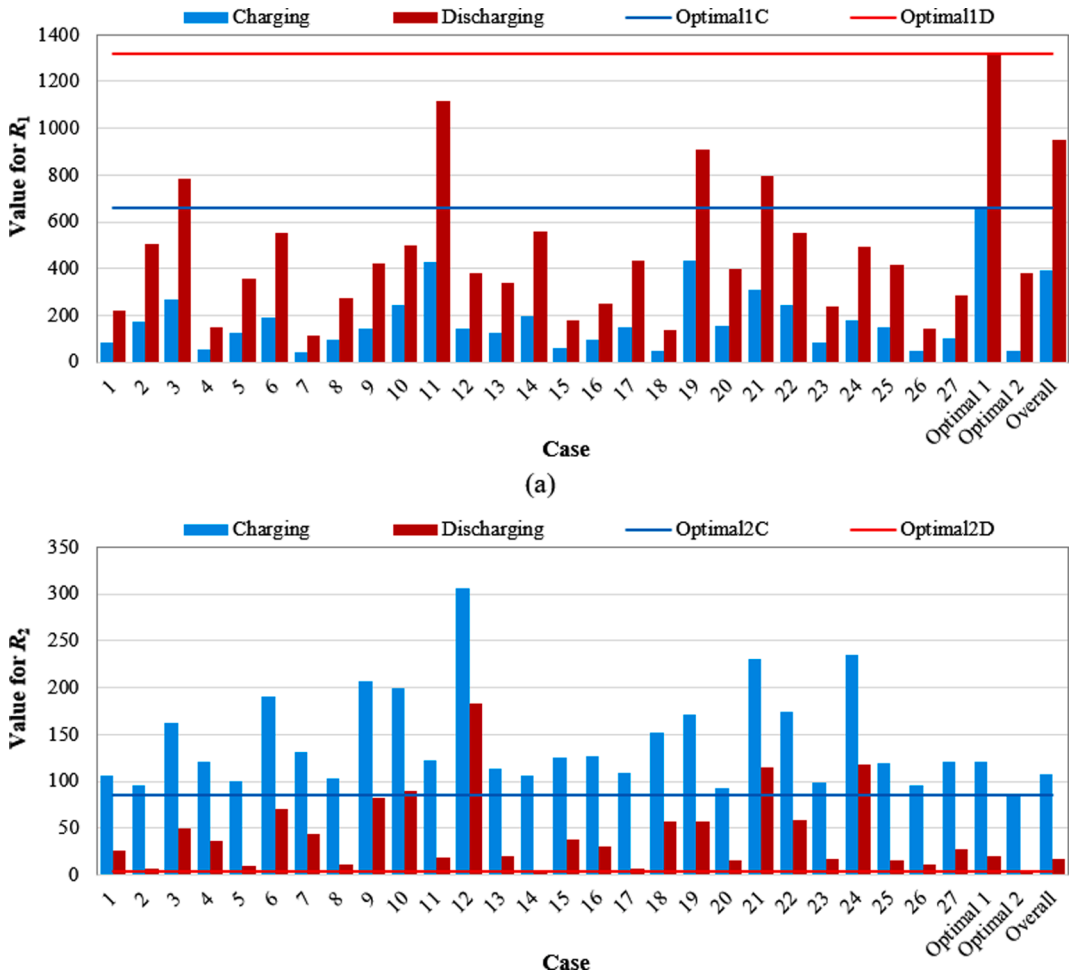

Fig. 11. Comparison of the results obtained using the investigated conditions (Table 4) and optimal conditions (Table 10) in terms of (a) R_1 and (b) R_2.

storage units using carbon dioxide as the phase change material, especially lacking a systematic parametric study on the design and operational parameters of thermal energy storage units. In this paper, an investigation was carried out on using carbon dioxide as the phase change material in a thermal energy storage unit for storing energy around −55 °C. A model of a pillow plate heat exchanger created in the Modelica language was used to establish a parametric study where both geometrical and operational parameters of the thermal energy storage were varied. The parametric study was conducted using design of experiments for both charging and discharging processes. The main findings of the study were the following:

- The recommended value for center-to-center plate distance was found to be 25 mm in all the cases. This value not only achieved the best thermal performance but also the lowest operational cost of the system.
- Aluminum was found to be the best plate material in all the cases. This was achieved due to the superior thermal properties of aluminum as compared to stainless steel. Moreover, aluminum costs less than copper and is less heavy, which means a lightweight heat exchanger. Nevertheless, application of aluminum in pillow plate heat exchangers has been limited in the literature, requiring further investigation. In particular, the suitability of using aluminum pillow plate heat exchangers for the pressure classes required in refrigeration systems has to be addressed.
- The best value for the difference between refrigerant saturation temperature and phase change temperature of the phase change material was found to be 15 °C. In this way, the highest driving force for heat transfer could be achieved, which shortens the phase change process, lowering the operational costs.
- Regarding the refrigerant flow rate, the lowest value of 4 kg/s was found to be the best both in terms of heat transfer and economic performances.

The results from the study will be used to identify the most promising operational and geometrical parameters for pillow plate thermal energy storage units. The optimal design and operating conditions of the thermal energy storage unit can be implemented in a full dynamic system model of a low-temperature refrigeration plant to investigate the effect of the storage on the overall system performance. Implementing this type of thermal energy storage units (presented in the current work) in the food processing industry can provide valuable flexibility for system owners as well as utility companies with respect to decoupling the demand and supply of cooling systems and avoiding power consumption during peak hours.

Declaration of Competing Interest

The authors declare that they have no known competing financial interests or personal relationships that could have appeared to influence the work reported in this paper.

Data availability

Datasets related to this paper can be found at https://doi.org/10.18710/QGK54K, an open-source online data repository hosted at

DataverseNO [53].

Acknowledgements

This study was carried out through the research project KSP PCM-STORE (308847) supported by the Research Council of Norway and industrial partners. PCM-STORE aims at building knowledge on novel PCM technologies for low and medium temperature thermal energy storage systems.

References

[1] D. Coulomb, J.-L. Dupont, A. Pichard, The Role of Refrigeration in the Global Economy-29. Informatory Note on Refrigeration Technologies, (2015).
[2] A. Mota-Babiloni, M. Mastani Joybari, J. Navarro-Esbrí, C. Mateu-Royo, Á. Barragán-Cervera, M. Amat-Albuixech, F. Molés, Ultralow-temperature refrigeration systems: configurations and refrigerants to reduce the environmental impact, Int. J. Refrig 111 (2020) 147–158.
[3] K. Panchabikesan, M. Mastani Joybari, F. Haghighat, U. Eicker, V. Ramalingam, Analogy between thermal, mechanical, and electrical energy storage systems, 2021.
[4] H. Selvnes, Y. Allouche, R.I. Manescu, A. Hafner, Review on cold thermal energy storage applied to refrigeration systems using phase change materials, Therm. Sci. Eng. Progress 22 (2021), 100807.
[5] M. Mastani Joybari, F. Haghighat, J. Moffat, P. Sra, Heat and cold storage using phase change materials in domestic refrigeration systems: the state-of-the-art review, Energ. Buildings 106 (2015) 111–124.
[6] J. Sun, M. Zhang, A. Gehl, B. Fricke, K. Nawaz, K. Gluesenkamp, B. Shen, J. Munk, J. Hagerman, M. Lapsa, COVID 19 vaccine distribution solution to the last mile challenge: experimental and simulation studies of ultra-low temperature refrigeration system, Int. J. Refrig. 133 (2022) 313–325.
[7] A. Sevault, F. Vullum-Bruer, O.L. Tranås, Active PCM-based thermal energy storage in buildings, in: L.F. Cabeza (Ed.), Encyclopedia of Energy Storage, Elsevier, Oxford, 2022, pp. 453–469.
[8] G. Li, Y. Hwang, R. Radermacher, H.-H. Chun, Review of cold storage materials for subzero applications, Energy 51 (2013) 1–17.
[9] D. Zheng, X. Wu, Comprehensive evaluation of eutectic character used as low temperature thermal energy storage, Gryogenics (2002).
[10] N. Guo, Thermal Properties Research of the Multivariate Organic Phase Change Materials for Cooling System, Chongqing University, Chongqing, 2008.
[11] E. Domalski, E. Hearing, Condensed phase heat capacity data, NIST Chemistry WebBook, NIST Standard Reference Database 69 (2005).
[12] J. Chickos, W. Acree, J. Liebman, Students of Chem 202 (Introduction to the Literature of Chemistry), University of Missouri–St. Louis,“ Heat of Fusion data” in: P.J. Linstrom, W.G. Mallard (Eds.), NIST Chemistry WebBook, NIST Standard Reference Database Number 69, National Institute of Standards and Technology, Gaithersburg MD, 2011, 20899.
[13] H. Yamaguchi, X.-D. Niu, K. Sekimoto, P. Nekså, Investigation of dry ice blockage in an ultra-low temperature cascade refrigeration system using CO_2 as a working fluid, Int. J. Refrig. 34 (2011) 466–475.
[14] H. Yamasaki, H. Yamaguchi, K. Hattori, P. Neksa, Experimental observation of CO_2 dry-ice behavior in an evaporator/sublimator, Energy Procedia 143 (2017) 375–380.
[15] H. Yamasaki, Ö. Kizilkan, H. Yamaguchi, T. Kamimura, K. Hattori, P. Nekså, Experimental investigation of dry ice cyclone separator for ultra-low temperature energy storage using carbon dioxide, Energy Storage 2 (2020) e149.
[16] A. Hafner, T.S. Nordtvedt, I. Rumpf, Energy saving potential in freezing applications by applying cold thermal energy storage with solid carbon dioxide, Procedia Food Sci. 1 (2011) 448–454.
[17] E.H. Verpe, I. Tolstorebrov, A. Sevault, A. Hafner, Y. Ladam, Cold thermal energy storage with low-temperature plate freezing of fish on offshore vessels, in: Proceedings of the 25th IIR International Congress of Refrigeration. Montréal, Canada, August 24-30, 2019, IIR, 2019.
[18] M. Mastani Joybari, H. Selvnes, A. Sevault, A. Hafner, Potentials and challenges for pillow-plate heat exchangers: state-of-the-art review, Appl. Therm. Eng. (2022), 118739.
[19] H. Selvnes, A. Hafner, H. Kauko, Design of a cold thermal energy storage unit for industrial applications using CO_2 as refrigerant, in: 25th IIR International Congress of Refrigeration Proceedings, IIR, 2019.
[20] H. Selvnes, Y. Allouche, A. Sevault, A. Hafner, A CFD analysis for the performance assessment of a novel design of plates-in-tank latent storage unit for freezing applications, in: 8th Conference on Ammonia and CO_2 Refrigeration Technologies, Proceedings, IIR, 2019.
[21] H. Selvnes, Y. Allouche, A. Sevault, A. Hafner, CFD modeling of ice formation and melting in horizontally cooled and heated plates, in: Eurotherm Seminar# 112-Advances in Thermal Energy Storage, Edicions de la Universitat de Lleida Lleida, Spain, 2019.
[22] H. Selvnes, V. Büttner, A. Hafner, Evaluation of a pillow-plate heat exchanger for a pump-circulated CO_2 refrigeration system, in: Proceedings of the 14th IIR-Gustav Lorentzen Conference on Natural Refrigerants, International Institute of Refrigeration, 2020.
[23] H. Selvnes, Y. Allouche, A. Hafner, Experimental characterisation of a cold thermal energy storage unit with a pillow-plate heat exchanger design, Appl. Therm. Eng. 199 (2021), 117507.
[24] H. Selvnes, Y. Allouche, A. Hafner, A cold thermal energy storage unit for CO_2 refrigeration using phase change material: first experimental results, in: 9th Conference on Ammonia and CO_2 Refrigeration Technologies Ohrid, R. Macedonia September 16-17, 2021 Proceedings, International Institute of Refrigeration, 2021.
[25] H. Selvnes, Y. Allouche, A. Hafner, C. Schlemminger, I. Tolstorebrov, Cold thermal energy storage for industrial CO_2 refrigeration systems using phase change material: an experimental study, Appl. Therm. Eng. (2022), 118543.
[26] PCM RT-LINE, in: Rubitherm Thecnologies GmbH. Available from: <https://www.rubitherm.eu/en/index.php/productcategory/organische-pcm-rt>.
[27] A. Sevault, E. Næss, Active latent heat storage using biowax in a central heating system of a ZEB living lab, in: Proceedings of the 14th IIR-Gustav Lorentzen Conference on Natural Refrigerants, IIR, 2020.
[28] CrodaTherm™ 37 | Energy Technologies, in: Croda Energy Technologies. Available from: <https://www.crodaenergytechnologies.com/en-gb/product-finder/product/1387-CrodaTherm_1_37>.
[29] A. Sevault, F. Bøhmer, E. Næss, L. Wang, Latent heat storage for centralized heating system in a ZEB living laboratory: integration and design, in: IOP Conference Series: Earth and Environmental Science, Vol. 352, IOP Publishing, 2019, p. 012042.
[30] A. Sevault, F. Vullum-Bruer, O.L. Tranås, Active PCM-based thermal energy storage in buildings, in: 14th Gustav Lorentzen Conference, Kyoto, Japan, December 6-9, 2020, 2020.
[31] M. Mastani Joybari, M.S. Hatamipour, A. Rahimi, F.G. Modarres, Exergy analysis and optimization of R600a as a replacement of R134a in a domestic refrigerator system, Int. J. Refrig. 36 (2013) 1233–1242.
[32] J.T. Luo, M. Mastani Joybari, K. Panchabikesan, F. Haghighat, A. Moreau, M. Robichaud, Parametric study to maximize the peak load shifting and thermal comfort in residential buildings located in cold climates, J. Storage Mater. 30 (2020), 101560.
[33] K. Siebeneck, W. Popov, T. Stefanak, S. Scholl, Pillow plate heat exchangers–investigation of flow characteristics and wetting behavior at single-flow conditions, Chem. Ing. Tech. 87 (2015) 235–243.
[34] N. Abas, A.R. Kalair, N. Khan, A. Haider, Z. Saleem, M.S. Saleem, Natural and synthetic refrigerants, global warming: a review, Renew. Sustain. Energy Rev. 90 (2018) 557–569.
[35] W.L. Luyben, Estimating refrigeration costs at cryogenic temperatures, Comput. Chem. Eng. 103 (2017) 144–150.
[36] M. Mastani Joybari, H. Selvnes, A. Hafner, A. Sevault, Cold thermal energy storage in solid-liquid transition of carbon dioxide: Investigating the possibility, in: 15th IIR-Gustav Lorentzen Conference on Natural Refrigerants (GL2022), Trondheim, Norway, June 13-15 2022, 2022.
[37] P. Fritzson, V. Engelson, Modelica—A unified object-oriented language for system modeling and simulation, in: European Conference on Object-Oriented Programming, Springer, 1998, pp. 67–90.
[38] N.C. Lemke, J.L. Lemke, J. Koehler, Secondary Loop System for Automotiv HVAC Units Under Different Climatic Conditions, (2012).
[39] S. Smitt, Á. Pardiñas, A. Hafner, Evaluation of integrated concepts with CO_2 for heating, cooling and hot water production, Energies 14 (2021) 4103.
[40] Á.Á. Pardiñas, M. Jokiel, C. Schlemminger, H. Selvnes, A. Hafner, Modeling of a CO_2-based integrated refrigeration system for supermarkets, Energies 14 (2021) 6926.
[41] A. Hafner, S. Försterling, K. Banasiak, Multi-ejector concept for R-744 supermarket refrigeration, Int. J. Refrig. 43 (2014) 1–13.
[42] S. Försterling, H. Selvnes, A. Sevault, Validation of a Modelica numerical model for pillow plate heat exchangers using phase change material, in: 15th IIR-Gustav Lorentzen Conference on Natural Refrigerants, June 13-15 2022, Trondheim, Norway, 2022.
[43] E. Lemmon, I.H. Bell, M. Huber, M. McLinden, NIST Standard Reference Database 23: Reference Fluid Thermodynamic and Transport Properties-REFPROP, Version 10.0, National Institute of Standards and Technology, Standard Reference Data Program, Gaithersburg, 2018.
[44] R. Span, W. Wagner, A new equation of state for carbon dioxide covering the fluid region from the triple-point temperature to 1100 K at pressures up to 800 MPa, J. Phys. Chem. Ref. Data 25 (1996) 1509–1596.
[45] M. Mastani Joybari, H. Selvnes, A. Sevault, A. Hafner, Replication Data for: Cold thermal energy storage in solid-liquid transition of carbon dioxide: Investigating the possibility, in: S. Norwegian University of, Technology (eds.), DataverseNO, 2022.
[46] H.D. Baehr, K. Stephan, Wärme-und stoffübertragung, Springer, 1994.
[47] J.G. Collier, J.R. Thome, Convective Boiling and Condensation, Clarendon Press, 1994.
[48] M.M. Shah, A general correlation for heat transfer during film condensation inside pipes, Int. J. Heat Mass Transf. 22 (1979) 547–556.
[49] P.K. Swamee, A.K. Jain, Explicit equations for pipe-flow problems, J. Hydraul. Div. 102 (1976) 657–664.
[50] Minitab 21 Statistical Software. [Computer software], State College, PA: Minitab, Inc. (www.minitab.com), 2022.
[51] M. Ghalambaz, S. Mehryan, A. Veismoradi, M. Mahdavi, I. Zahmatkesh, Z. Kazemi, O. Younis, M. Ghalambaz, A.J. Chamkha, Melting process of the nano-enhanced phase change material (NePCM) in an optimized design of shell and tube thermal

energy storage (TES): Taguchi optimization approach, Appl. Therm. Eng. 193 (2021), 116945.

[52] A.N. Mustapha, Y. Zhang, Z. Zhang, Y. Ding, Q. Yuan, Y. Li, Taguchi and ANOVA analysis for the optimization of the microencapsulation of a volatile phase change material, J. Mater. Res. Technol. 11 (2021) 667–680.

[53] M. Mastani Joybari, H. Selvnes, E. Vingelsgård, A. Sevault, A. Hafner. Replication Data for: Parametric study of low-temperature thermal energy storage using carbon dioxide as the phase change material in a pillow plate heat exchanger, Norwegian University of, Technology (eds.), DataverseNO, 2022.